Check for updates

Received: 19 August 2020 | Revised: 1 October 2020 | Accepted: 21 October 2020

DOI: 10.1002/er.6188

RESEARCH ARTICLE

INTERNATIONAL JOURNAL OF ENERGY RESEARCH WILEY

Tunable current duration in triboelectric generators via capacitive air gaps

Byungseok Seo[1] | Youngsun Cha[1] | Sangtae Kim[2] | Wonjoon Choi[1]

[1]School of Mechanical Engineering, Korea University, Seoul, South Korea

[2]Department of Nuclear Engineering, Hanyang University, Seoul, South Korea

Correspondence
Sangtae Kim, Department of Nuclear Engineering, Hanyang University, Seoul 04763, South Korea.
Email: sangtae@hanyang.ac.kr
Wonjoon Choi, School of Mechanical Engineering, Korea University, Seoul, 02841, South Korea
Email: wojchoi@korea.ac.kr

Funding information
Hanyang University, Grant/Award Number: HY- 202000000000524; Korea Institute of Energy Technology Evaluation and Planning (KETEP) and the Ministry of Trade, Industry & Energy (MOTIE), Grant/Award Number: 20173010032170; National Research Foundation of Korea, Grant/Award Numbers: 2019R1A2C2085583, 2020R1A5A1018153

Summary

Despite the low cost, high power, and wide application areas, impact-type triboelectric generators exhibit limited applicability due to the extremely short current duration, on the order of a millisecond. The high power, short lasting current peak not only results in reduced time-averaged power output but also acts as triboelectric shock to the accompanying circuits, quickly degrading the usability of the generator. Here, we demonstrate tunable triboelectric current duration via controlling the air gap capacitance inserted between the two dielectric plates. In typical contact-type triboelectric generator with nylon/air gap/Polydimethylsiloxane (PDMS) multilayers, decreasing the vertical speed of the dielectric plates from 0.5 cm/s to 0.05 cm/s result in increased current duration from 0.10 second to 0.81 second. The increased peak duration accompanies decreased peak current, resulting in the optimal charge density of 0.163 nC/cm^2 at the vertical speed of 0.25 cm/s. Changing the air gap capacitance in noncontact mode or the relative permittivity in dielectric layers also results in similar change in peak duration. To explain the tunable current duration, an equivalent circuit model is constructed via serially connected capacitors and numerical solutions reproduce the trends in current duration associated with change in air gap capacitance. This study provides significant implications toward further optimizing triboelectric generators, in terms of optimal triboelectric charge density, accompanying circuit lifetime and broadened applicability.

KEYWORDS

air gap capacitance, current duration, nanogenerator, time-averaged energy efficiency, triboelectricity

1 | INTRODUCTION

Over the past decade, efficient energy harvesters based on triboelectricity has garnered a significant research attention,[1,2] with potential applications in mobile electronics[3,4] and self-powered Internet of Things (IoT) platforms.[5,6] Triboelectric generators exploit the surface polarization induced upon touching two distinct surfaces, with key materials parameters including dielectric permittivity and relative triboelectric tendency.[7] Numerous studies have proposed power-enhancing strategies for triboelectric generators via optimizing surface charging behavior,[8,9] enhancing the dipole properties[10,11] or hybridizing with other energy harvesting mechanisms.[12,13] Yet, most of these studies focus on enhancing the peak power output, and the duration of triboelectric current remains severely limited to the order of millisecond timescale.[14]

 © 2020 John Wiley & Sons Ltd

The capability to tune the triboelectric current duration implies several critical technological advances. The amount of triboelectric charge generated scales with the current duration, pointing to the need for accessing the timescale axis in the optimization space. Also, extended triboelectric current duration may significantly ease the burden imposed on the charge collecting circuit connected to the generators. The irregular triboelectric current pulses require various circuit elements such as rectifiers, capacitor charging circuits, and impedance matching circuits.[15-18] The circuit elements, however, accumulate damages from triboelectric "shocks" of high peak, short lasting current pulses. The harsh environment for the circuit makes it difficult to reliably match the high impedance of triboelectric generators or collect the generated charges efficiently, when the mechanical input involves a wide range of input amplitudes and frequencies. Although the capability to tune the triboelectric current duration is much desired in terms of energy optimization and circuit lifetime, such capability has never been realized for impact type triboelectric generators.

To overcome this challenging situation, researchers have devised smart device geometry and mechanisms, such as hybridizing with other mechanisms of different natural frequency,[19] designing triboelectric generators in the electrostatic breakdown regime via rotating or moving dielectric layers,[20] or coupling with ion-gel printed capacitors.[21] While the rotating dielectric layer indeed results in continuous current output, a continuously rotating environment may impose optional constraints on some applications. Furthermore, other methods could not provide rational design guidelines, which overcome the short duration in power generation based on the impact-type triboelectricity.

In this work, we systematically study the change in current peak duration with respect to the device design parameters such as the dielectric layer speed during impact, maximum air gap distance between the two dielectrics and the effect of dielectrics combination (Figure 1A,B). The experiments show that the triboelectric current peak duration may be tuned by controlling the air gap capacitance, with the demonstrated current

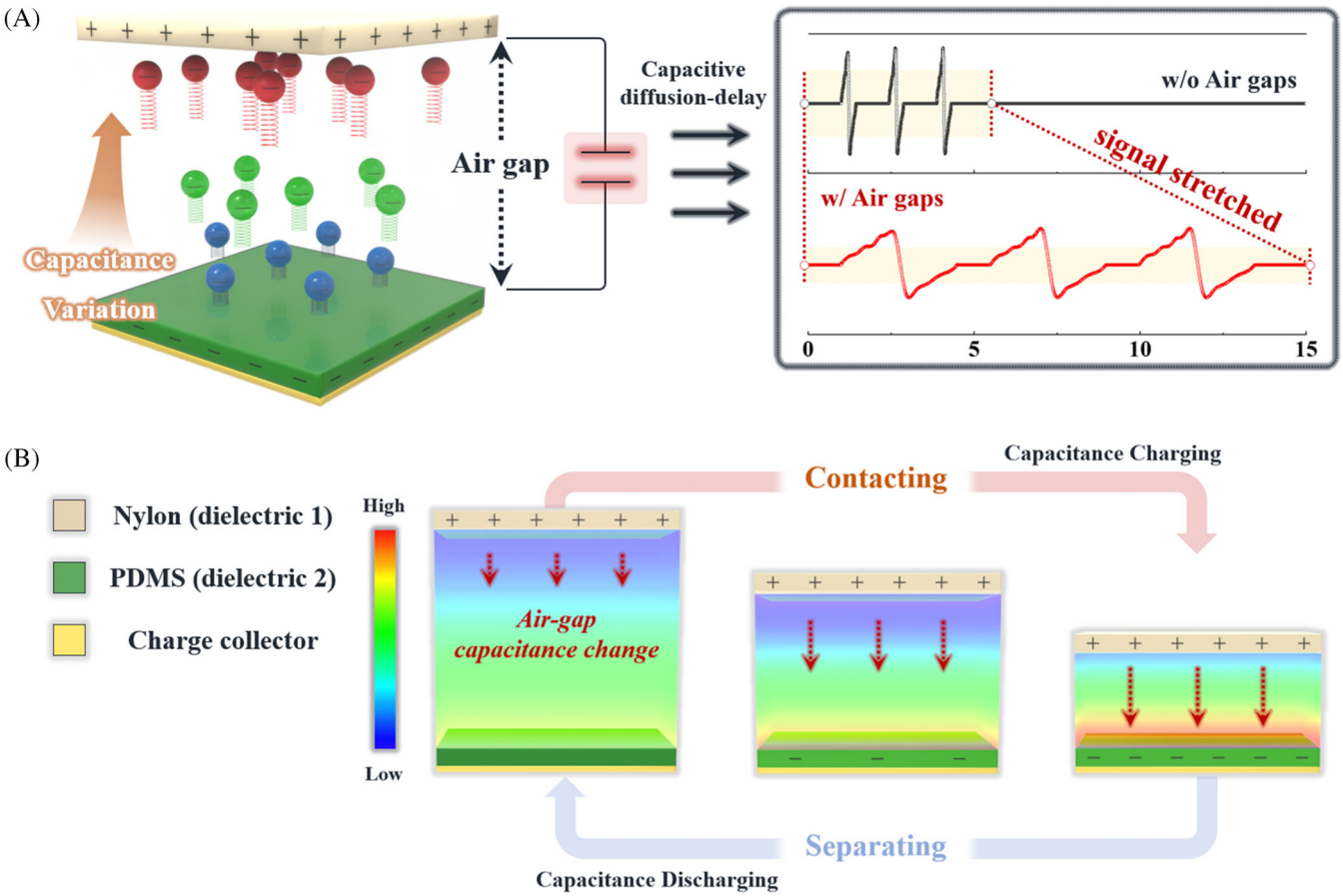

FIGURE 1 Schematics on the effect of air gap capacitance on triboelectric currents. (A) Conceptual illustrations on the tunable current peak widths via air gap capacitance. (B) Schematics on the experimental device configuration and cyclic triboelectric current generation [Colour figure can be viewed at wileyonlinelibrary.com]

duration between 0.1 and 0.8 seconds. Analytical expressions and equivalent circuit models have been derived, explaining the relation between current duration and air gap capacitance. These systematic studies suggest that the duration of triboelectric current peaks may be tuned up to 1 second, implying the potential design guidelines toward engineering the time-averaged efficiency according to the specific target motions. Such effort may open up the unexplored optimization space in terms of mechanical input frequency for impact-type triboelectric generators.

2 | EXPERIMENTAL METHODS

2.1 | Triboelectric device preparation consisting of dielectrics/air gap/dielectrics layers

Polyethylene terephthalate film of 20 μm thickness was cleaned by acetone and deionized water and used as the bottom substrate of TE. Double-sided adhesive tapes with high electrical conductivity (Solueta inc, SDC-30, 0.3 Ω) were applied on the substrate as current collectors, ensuring solid adhesion between the dielectrics and substrate surfaces. Polydimethylsiloxane (PDMS, Dow corning, Sylgard 184) layer was prepared by mixing its solution with curing agent via vortex mixer (DAIHAN, Multifunction Vortex Mixer, VM-10) at 10:1 weight ratio. The mixed PDMS solution (5 g) was then spin coated on the substrate at 120 rpm for 45 seconds, followed by an annealing procedure in baking oven at 80°C for 2 hours. The top dielectrics layer of free-standing nylon or polytetrafluoroethylene (PTFE) films were prepared with varied materials properties for triboelectricity (TE) (4 × 4 cm) and fixed to the moving parts of cam structure by screws. The thickness of all dielectric layers was fixed as 2 mm.

2.2 | Triboelectric test platform configuration

The test platform for triboelectric performance was built based on cam structures. The test device consists of a DC motor, gear components, and cam structure for vertical movements (Figure S1). The DC motor was powered by an external power supply (Keithley, 2200-30-5, 30 V, 5 A) and connected to gear components for force transmission. The vertical speed of the top dielectrics layer was controlled from 0.05 to 0.5 cm/s by the DC power. The height of the bottom dielectrics was adjusted by lifting the support jack, and the distance between the two dielectrics layers was controlled between 0 and 35 mm. The output current of the TE device was measured by digital phosphor oscilloscopes (Tektronix, DPO2004B) and digital multi-meter (Agilent 34464A) with external load of 1 MΩ serially connected to the triboelectric device. The digital multi-meter measurements were performed with an number of power line cycles (NPLC) of 0.02 to ensure sufficient sampling of the current output.

2.3 | Modeling and analysis via equivalent circuit formation

The equivalent circuit model based on capacitance was designed to obtain an analytical expression for parametric study and estimation of current profiles. The displacement of the top dielectrics was assumed to be a one-dimensional linear function of time. According to the Gaussian theorem, the electric fields between the dielectrics and the air gap were obtained, and the electric potential of each component in the closed circuit was obtained by Kirchhoff's voltage law (KVL). The governing equations for the total charge generated (Q) and the triboelectric current output (dQ/dt) were derived based on Ohmic behavior, and the resultant current profiles according to time were numerically evaluated using Dawson integral. The current behavior according to major parameters for charge diffusion such as stimuli speed, air gap size, and the permittivity of dielectrics are analyzed, as well as the correlation between them.

3 | RESULTS AND DISCUSSION

3.1 | Triboelectric current peak widths according to the dielectric speed in nylon/air gap/PDMS

Upon repetitive mechanical input, contact-mode triboelectric generators produce alternating current signals. For efficient analysis of the current signals, we designate two major parameters for determining the shape of the current signal, the instantaneous peak current and peak width (Figure 2A). Specifically, the time it takes for I_{peak} to decay up to 63.2% $(1-\frac{1}{e}=0.632)$ is defined here as the peak width.

Figure 2B shows the current response according to the dielectric layer's vertical speed, with the fixed maximum air gap size. As the vertical speed increases from 0.05 and 0.5 cm/s, the peak current sharply increases from 1.11 to 10.9 nA. At the same time, the peak widths decrease from 0.81 second to 0.10 second upon the same speed increase. Interestingly at 0.05 cm/s speed, the current profile exhibits continuous increase for approximately 1.5 seconds until it hits the peak value, followed

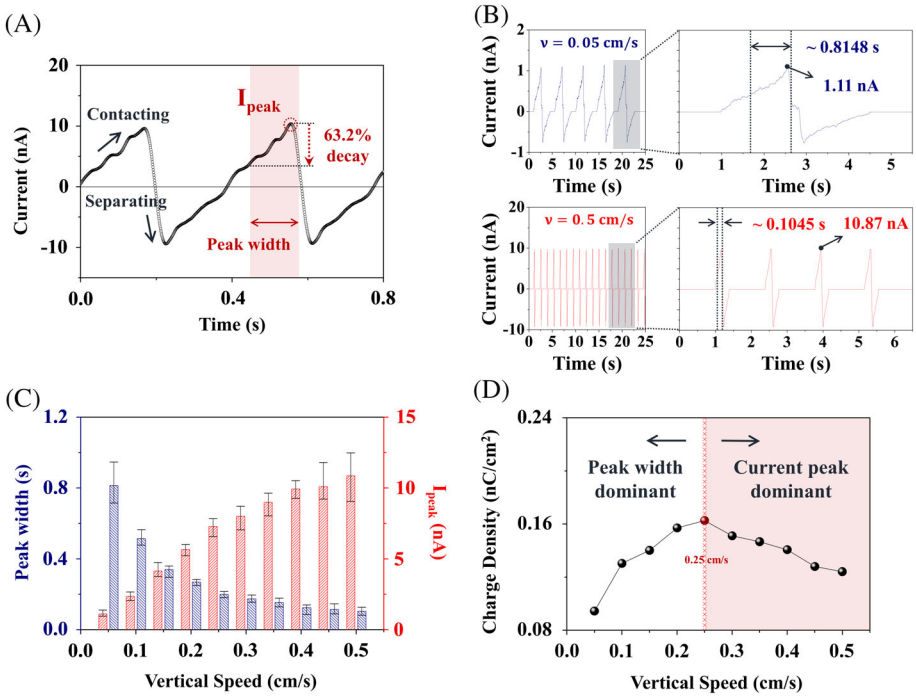

FIGURE 2 The triboelectric current characteristics generated from nylon/PDMS dielectrics with varied vertical speed. (A) A representative triboelectric current signal after noise filtering with the definitions of the peak current and peak widths. (B) The difference in triboelectric current characteristics for the upper dielectric plate's vertical speed of 0.05 and 0.5 cm/s. (C) The peak current and peak widths of the triboelectric current peaks according to vertical speeds. (D) The amount of triboelectric charge density generated according to the vertical speed for a single triboelectric cycle [Colour figure can be viewed at wileyonlinelibrary.com]

by a sharp decay (Figure S2a). Similar trends are observed for the other vertical speeds, just at different overall timescales (Figure S2b-d). The trend among peak current, peak widths, and vertical speed persists monotonically among the vertical speeds between 0.05 and 0.5 cm/s (Figure 2C). The increase in peak width reaches up to 780%, while the decrease of the current peak up to 979%, upon the speed increase from 0.05 to 0.5 cm/s. The rate of change according to duration (slope of Figure 2C) is the largest at 0.05 cm/s for both the peak width and peak current, with slow saturation behavior as the speed increases above 0.2 cm/s. The peak current also exhibits the sharpest increase in the slow speed regime, with signs of saturation at 0.5 cm/s. It is noted that the peak width of 0.10 second is yet considerably larger than those typically reported in the literature and is caused by the intentional sampling rate that focuses on capturing the overall shape of the current peaks, rather than the sharp peak current. Such sampling rate first ensures that we obtain a current peak free of noise from the surrounding environment, and second allows us to obtain a current signal that captures the time-averaged output on the order of 0.01 seconds. The sampling scheme neglects the sharp triboelectric peak current with typical peak widths of ~1 millisecond, yet allows accurate assessment of the generated charge and peak widths. We believe this is appropriate when we target observing the change in the overall behavior of the current output upon vertical speed or air gap thickness change, which occurs in the timescales on the order of 1 seconds.

Interestingly, the triboelectric charge density generated at different speed exhibits an optimal speed during the peak height peak width trade-off. Figure 2D shows that the maximum triboelectric charge of 0.163 nC/cm^2 is generated at 0.25 cm/s, below which low peak heights result in low overall charge generation and above which low peak widths lead to reduced charge density. As the time duration of exchanging charges between dielectrics and air was elongated, the dissipated energy amount can be reduced due to system stabilization, and it induced increase of peak current complement (Figure S3). The rate of decrease for charge density appears slightly higher in the slow speed regime, with noticeably increased signal noises (Figure S4).

3.2 | The effect of air gap thickness to triboelectric current in noncontacting mode

To elucidate whether the thick air gaps induce the change in current peak characteristics, we evaluate the effect of air gap thickness at the fixed speed of 0.05 cm/s. The air gaps are controlled by varying the minimum distance between the two dielectric layers during operation; the minimum distance of 0 mm indicates contact/separation mode and the others noncontact mode (inset image of Figure 3A). At the same vertical speed, increasing the air gap thickness results in reduced peak current, while the peak widths increase (Figure 3A). The increase in

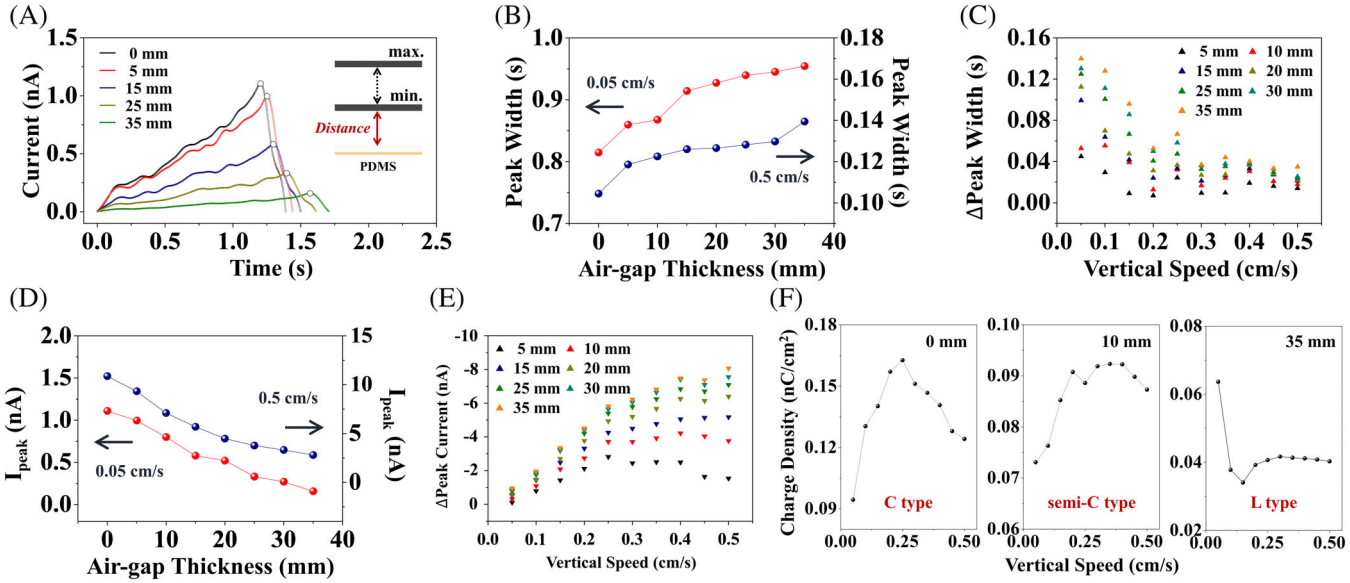

FIGURE 3 Triboelectric current characteristics for noncontact mode operation of nylon/PDMS-based generator. (A) Change in current peak profiles according to the air gap spacing inserted for noncontact mode operation. The air gap spacing stands for the minimum distance between the top and bottom dielectrics (inset image) at a constant vertical speed of 0.05 cm/s. (B) The peak widths according to the inserted air gap thickness at two different vertical speeds of 0.05 and 0.5 cm/s. (C) The change in peak widths according to the inserted air gap spacing and vertical speed in the noncontact mode operation. (D, E) The change in peak current according to the inserted air gap thickness and vertical speed. (F) Three distinct behavior of triboelectric charge density according to the vertical speed at different air gap distance inserted. As the air gap spacing in the noncontact mode increases, the optimal behavior in TE charge density changes dramatically [Colour figure can be viewed at wileyonlinelibrary.com]

peak widths with respect to increasing air gap distance persists for most vertical speeds tested (Figure 3B). At the speed of 0.5 cm/s, the peak widths increase from 0.105 to 0.139 second. The extent in the peak width increase is notably smaller than that at 0.05 cm/s from 0.815 to 0.955 second. Figure 3C plots the change in peak widths with respect to the contact mode peak widths according to the vertical speed and air gap distance. Generally, increasing the vertical speed reduces the variance in peak widths, with only small change in peak widths of approximately 0.03 second observed at 0.5 cm/s speed. The largest change in peak widths observed reaches 0.135 second at 0.05 cm/s speed and 35 mm air gap thickness. Most experiments in previously developed triboelectric generators have been performed at vertical speeds exceeding 1 cm/s, and thus the change in peak widths has not been observable.[22-24]

The peak current exhibits the opposite trend to the peak widths according to the air gap distance. As the air gap distance increases, the peak current monotonically decreases for all vertical speeds tested between 0.05 and 0.5 cm/s. At 0.5 cm/s speed, the peak current decreases by 74.2% from 10.87 to 2.86 nA, as the air gap distance increases from 0 to 35 mm. At 0.05 cm/s speed, the decrease in peak current reaches 85.6% from 1.11 to 0.16 nA. The trend is understood in terms of the decreasing amount of triboelectricity upon increasing air gap thickness. The similar trend in peak current decrease among varied vertical speed suggests that the physics behind peak current decrease is identical despite varied air gap thickness. Plotting the decrease in current with respect to vertical speed at all air gap distances tested reveal that the absolute amount of decrease in peak current increases significantly with vertical speed, despite the monotonic trend. For instance, the absolute amount of decrease in peak current at 0.05 cm/s is far less than that at 0.5 cm/s as the air gap thickness decreases from 35 to 5 mm. This is the opposite to the trend in peak widths, suggesting that an optimal value may exist in terms of total charge generated.

Figure 3F compares the total triboelectric charge generated (the area under a current peak) with respect to the vertical speed at three different air gap thickness. In the contact mode (air gap thickness of 0 mm), there exists an optimal vertical speed identical to Figure 2D. In noncontact modes, the behavior exhibits a cross over as the air gap thickness increases. At 10 mm air gap thickness, the highest charge density is generated around the optimal vertical speed in contact mode, with the optimal value spread around larger vertical speed. This suggests that the trade-off relation persists in noncontact mode with small air gap distance, with greater contribution

from peak current to the charge density. At 35 mm air-gap, the maximum charge density dominantly occurs at 0.05 cm/s vertical speed, with a sharp decrease for most other vertical speeds. At this large air gap thickness, the increased current peak width dominates the charge generation, clearly demonstrating the cross over in dominant charge generating mechanism. The cross-over in this specific case occurs between 15 mm and 20 mm air gap thickness (Figure S5).

3.3 | Equivalent circuit model for triboelectric current generation

An equivalent circuit model is established to understand the origin of the peak width tuning according to the the vertical speed and air gap distance (Figure 4A). The circuit is constructed assuming a double-electrode model, since the one-electrode model involves an open circuit to the ground.[25-27]

Assuming that the PDMS layer stays still, the maximum height and movement range of nylon layer are designated as x_{max} and x_{fluct}, respectively. When the two dielectrics periodically touch each other in contact mode, x_{max} equals x_{fluct}. Defining the distance from the surface of PDMS as $x(t)$, we obtain the following simple expression for the air gap size assuming linear displacement profiles (Figure S6):

$$\text{Separating}: x(t) = \nu t + (x_{max} - x_{fluct}) \quad (1)$$

$$\text{Approaching}: x(t) = -\nu t + x_{max} \quad (2)$$

Here, ν stands for the fixed movement speed. Using Gauss law on the equivalent circuit in Figure 4B, the electric fields (E) distributed within the triboelectric generator is written as

$$E_{nylon} = -\frac{Q}{S\varepsilon_0\varepsilon_{nylon}},\ E_{air-gap} = \frac{-\frac{Q}{S}+\sigma}{\varepsilon_0},\ E_{PDMS} = -\frac{Q}{S\varepsilon_0\varepsilon_{PDMS}} \quad (3)$$

where ε_0 stands for the vacuum permittivity, ε_{nylon} and ε_{PDMS} the relative permittivity of nylon and PDMS, Q the total charge, S the surface area of the thin film dielectrics, and σ the surface charge density. KVL reveals the electric potential (V) across the capacitance, where d is the thickness of dielectrics:

$$V = E_{nylon}d_{nylon} + E_{PDMS}d_{PDMS} + E_{air-gap}x(t) \quad (4)$$

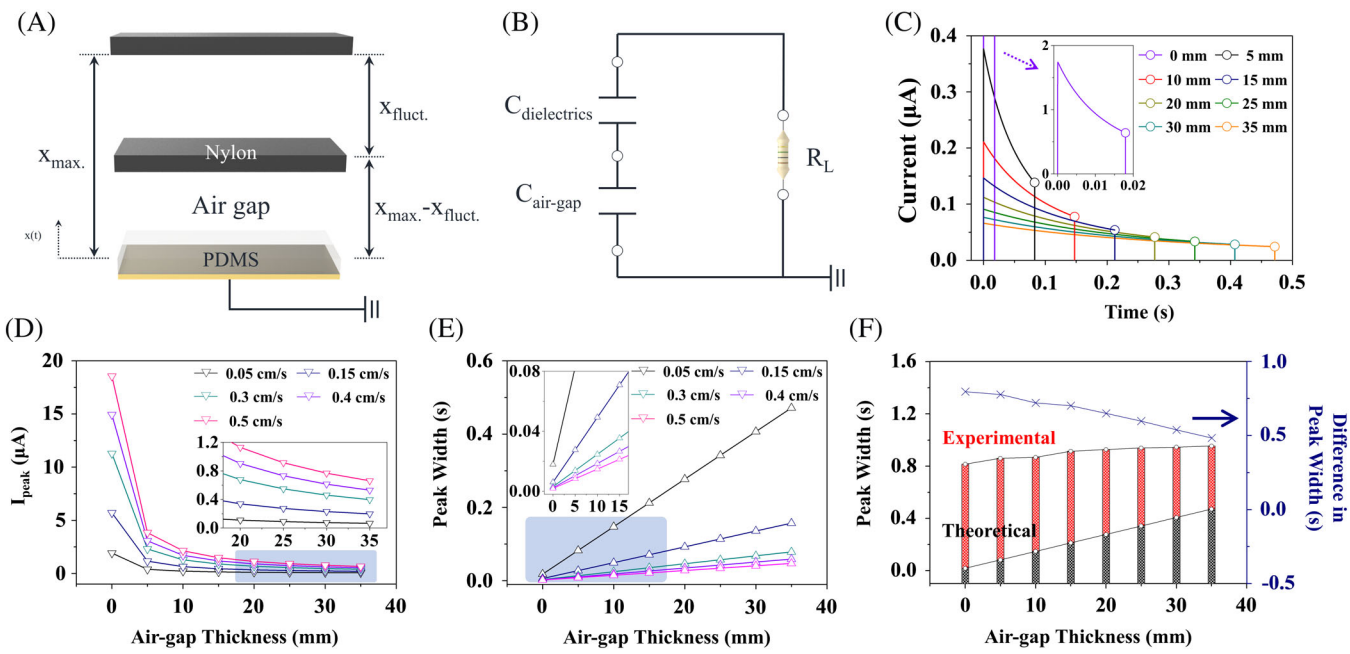

FIGURE 4 Equivalent circuit model based on two capacitors and a resistor for the triboelectric generator. (A) The geometric depiction and (B) the equivalent circuit model for the nylon/air gap/PDMS triboelectric generator. (C) The numerically solved current profiles at the fixed vertical speed of 0.05 cm/s and varied air gap spacing of 0, 5, 10, 15, 20, 25, 30, and 35 mm. The resultant (D) peak current and (E) peak widths according to the air gap spacing and the vertical speed for the numerically solved equivalent circuit model. (F) Comparison between the numerical and experimental results of peak widths at the vertical speed of 0.05 cm/s [Colour figure can be viewed at wileyonlinelibrary.com]

$$V = \frac{-Q}{S\varepsilon_0}(d_0 + x(t)) + \frac{\sigma x(t)}{\varepsilon_0}, d_0 = \frac{d_{\text{nylon}}}{\varepsilon_{\text{nylon}}} + \frac{d_{\text{PDMS}}}{\varepsilon_{\text{PDMS}}} \tag{5}$$

Applying Ohm's law across the closed circuit, the equation can be written as a first-order ordinary differential equation in terms of charge (Q) with respect to time (t):

$$R_{\text{L}}\frac{\text{d}Q}{\text{d}t} = -\frac{Q}{S\varepsilon_0}(d_0 + x(t)) + \frac{\sigma x(t)}{\varepsilon_0} \tag{6}$$

Inserting (5) into (6), we obtain the following.

$$R_{\text{L}}\frac{\text{d}Q}{\text{d}t} = -\frac{Q}{S\varepsilon_0}\left(\frac{d_{\text{nylon}}}{\varepsilon_{\text{nylon}}} + \frac{d_{\text{PDMS}}}{\varepsilon_{\text{PDMS}}} + (2\nu t + (x_{\max} - x_{\text{fluct}}))\right) + \frac{\sigma(2\nu t + (x_{\max} - x_{\text{fluct}}))}{\varepsilon_0} \tag{7}$$

Setting the appropriate initial condition $Q(t = 0) = 0$, the total charge generated can be expressed as the following:

$$\begin{aligned} Q(t) = \sigma S - \sigma S \exp\left[-\frac{1}{R_{\text{L}}S\varepsilon_0}\left(d_0 t + \int_0^{\tau} x(t)\text{d}t\right)\right] \\ - \frac{\sigma d_0}{R_{\text{L}}\varepsilon_0}\exp\left[-\frac{1}{R_{\text{L}}S\varepsilon_0}\left(d_0 t + \int_0^{\tau} x(t)\text{d}t\right)\right] \\ \times \int_0^t \exp\left[\frac{1}{R_{\text{L}}S\varepsilon_0}\left(d_0 z + \int_0^z x(z)\text{d}z\right)\right]\text{d}z \end{aligned} \tag{8}$$

Current profile for each separating segment can be obtained by differentiating (8) with respect to time:

$$\begin{aligned} I(t) = \frac{\text{d}Q}{\text{d}t} = -\frac{\sigma d_0}{R_{\text{L}}\varepsilon_0} + \frac{\sigma(d_0 + x(t))}{R_{\text{L}}\varepsilon_0}\exp\left[-\frac{1}{R_{\text{L}}S\varepsilon_0}\left(d_0 t + \int_0^{\tau} x(t)\text{d}t\right)\right] \\ + \frac{\sigma d_0}{R_{\text{L}}\varepsilon_0} \times \frac{d_0 + x(t)}{R_{\text{L}}S\varepsilon_0}\exp\left[-\frac{1}{R_{\text{L}}S\varepsilon_0}\left(d_0 t + \int_0^{\tau} x(t)\text{d}t\right)\right] \\ \times \int_0^{\tau} \exp\left[\frac{1}{R_{\text{L}}S\varepsilon_0}\left(d_0 z + \int_0^z x(z)\text{d}z\right)\right]\text{d}z \end{aligned} \tag{9}$$

The materials properties and fitting constants are organized in Table S1. The detailed derivation is organized in Note S1 (Supplementary Information).

Using the equivalent circuit model and the derived expressions for the triboelectric current, we plot the modeled current peak widths with respect to the air gap thickness at the fixed vertical speed of 0.5 cm/s in Figure 4C. The peaks are plotted up to their peak widths (the point at which the peak current decays up to 63.2%) for visual clarity. As the air gap thickness increases from 0 mm, to 35 mm, the peak current decreases from 1.74 to 0.066 μA. At the same time, the peak widths increase from 0.018 to 0.47 second. Solving the model above at various vertical speeds and air gap thickness, we obtain the current profiles for different combinations (Figure S7). The general trend in peak currents and peak widths is reproduced with varied air gap thicknesses and vertical speeds, with increasing air gap thickness, the variance in peak current decreases while the variance in peak widths increases (Figure 4D,E). In addition, the model predicts a linear relation between peak widths and air gap distances for all vertical speeds between 0.05 and 0.5 cm/s, similar to the experimentally observed variation in peak widths (Figure 3B). Notably, the decrease in peak current according to the air gap thickness is much more severe in modeled currents than observed in experiments, with exponential-like decay in the modeled currents compared to almost linear decay in the experimental currents. Also, the peak widths are modeled to be significantly less than the experimentally measured peak widths, with the gap in peak widths widening especially in small air gap thickness region (Figure 4F). The gap ranges between 0.48 second at 35 mm and 0.80 second at 0.05 cm/s speed.

There may be several reasons for this difference between the modeled and experimentally measured current peaks. An obvious source of error is the insufficient sampling of the current peaks, leading to the inaccurate measurement of the current peak widths. The large overall peak widths especially in small air gap and contact modes support this notion. The underestimation of peak current in the contact mode for all speeds may also be understood in terms of insufficient sampling rate. As the limited sampling rate overestimates the current peak widths, the instantaneous peak current gets averaged into underestimated current peak with overestimated peak widths. In the case of total charge generation, the output current derived by numerical modeling yielded approximately identical results (Figure S8), which was discorded with the experimental results (Figure S9), according to the air gap distance. This phenomenon is because Kirchhoff's law was applied in the process of estimating the electric potential across the capacitance layers in numerical modeling, and there is an inherent assumption that total charge generation must be conserved. In this sense, the model cannot predict or explain the optimal vertical speed and air gap thickness that maximizes the total triboelectric charge generated.

3.4 | The effect of dielectric layer's relative permittivity on the current characteristics

To examine whether the tunable current peak widths are observed with different dielectric materials, we perform

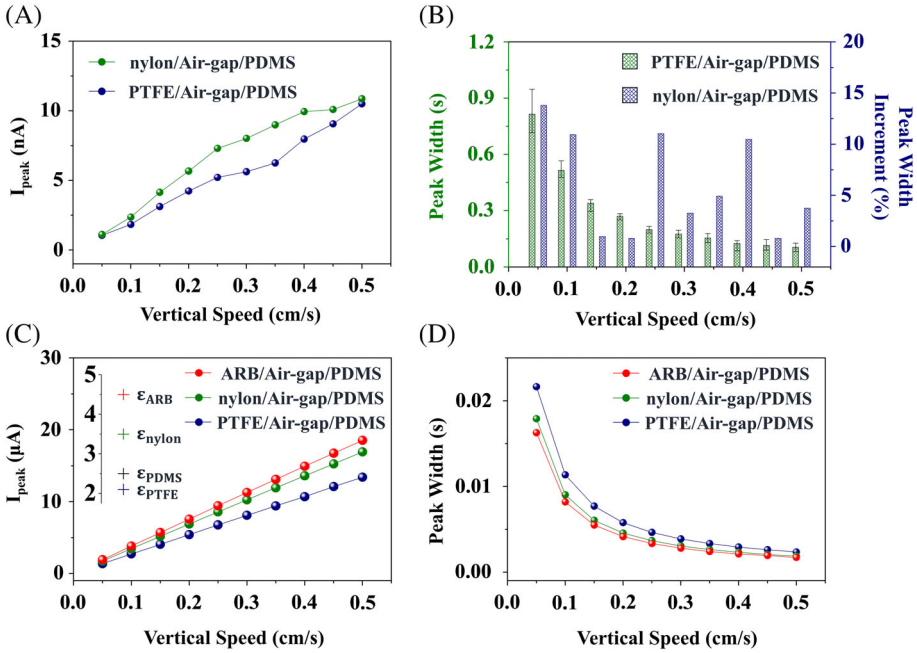

FIGURE 5 The effect of dielectric layers on the triboelectric charge generation. Experimental (A) peak current and (B) peak widths at varied vertical speed for two distinct combination of dielectric layers, nylon/PDMS and PTFE/PDMS. Numerically estimated (C) peak current and (D) peak widths according to the vertical speed for three distinct combinations with the specified relative permittivity in the inset. ARB stands for arbitrary dielectric layer with the relative permittivity value of 4.5 [Colour figure can be viewed at wileyonlinelibrary.com]

similar experiments with a different combination of dielectric materials, at the same geometric dimensions. The tested pair employs PTFE against PDMS. PTFE is intentionally chosen to make PDMS the more positive electrode since PTFE lies on the more negative side compared to PDMS on the triboelectric series. This contrasts PDMS being the negative side against nylon in the above experiments.

Figure 5a shows that the peak triboelectric current decreases up to 21.6% when employing PTFE-PDMS combination, compared to Nylon-PDMS combination, reflecting the smaller difference in triboelectric tendency. The peak duration, however, increases overall up to 13.8% (Figure 5b), with similar general tendency of decreasing peak duration with respect to increasing vertical speed. In efforts to quantify the effect of the dielectric constant on the peak duration, we estimate the peak current and current duration obtained from the equivalent circuit model above and plot them for three different dielectric constants, namely an arbitrary dielectric (ARB), nylon, and PTFE. The relative permittivity for the three are 4.5, 3.5 and 2.1, respectively (Table S1). Similar to the experiments, peak current increases with increasing difference in relative permittivity between the two dielectrics, while the time duration decreases. In ARB/air gap/PDMS, the peak current increases by 39.4% on average while the peak duration decreases by 27.4%, compared to PTFE/air gap/PDMS combination. Nylon/air gap/PDMS combination involves 26.9% increase in peak current and 20.5% decrease in peak duration, compared to PTFE/air gap/PDMS combination. The results above show that the combination of the dielectric layers affect the overall dielectric constants, although the effects are not as significant as that by the air gaps.

The implications of the tunable current duration in impact-type triboelectric generators are substantial. Contrast to piezoelectric generators, triboelectric generators suffer from lack of resonance frequency, at which the generated power output gets maximized. This owes to the fact that the native peak widths of triboelectric generators are very small (on the order of 1 millisecond) and that the triboelectric generators also require sufficient final spacing between the two dielectric plates (the maximum distance between the two plates) for sufficient power output. While increasing the mechanical input frequency enhances the time-averaged power output due to the number of increasing power peaks, reducing the maximum distance at the same time decreases the power output. The capability to tune the overall peak shape of the triboelectric generators, thus implies that a triboelectric generator may be tuned to specific frequency motion for optimized power output, much like resonance tuning in piezoelectric generators. Despite the small power output, we have demonstrated that there exists an optimal vertical speed at which the charge generation becomes maximized, and such speeds may be realized in impact-type devices by employing vertical spring components that control the motions of the dielectric plates.

4 | CONCLUSION

In this work, we demonstrate that the triboelectric peak duration of a typical impact-type triboelectric generator

can be tuned via controlling the vertical speed of the dielectric, air gaps inserted between dielectrics, or the combination of the dielectric materials. In a simple nylon/air gap/PDMS multilayer generator, the peak duration increases by up to 780% when the dielectric layer's vertical speed decreases from 0.5 cm/s to 0.05 cm/s. This increase in peak duration is accompanied by the decrease in peak current by up to 979%. This competing behavior suggests an optimization behavior in the generated triboelectric charges, and the maximum triboelectric charge density value of 0.163 nC/cm^2 has been obtained at the speed of 0.25 cm/s. The triboelectric current duration may also be increased by inserting air gap between the dielectric plates and operating in noncontact mode. Introducing the air gap of 35 mm results in the increased peak duration of 0.14 and 0.035 second compared to contact modes, at 0.05 and 0.5 cm/s vertical speeds, respectively. We explain the increase in peak duration with an equivalent circuit model, and numerical solutions reproduces the experimentally observed trends. The different dielectric layers and thus the relative permittivity also affect the peak duration, although not as much as the other two variables. The tunable triboelectric peak currents demonstrated in this study provides potential improvement of triboelectric generators toward more durable and powerful energy harvesters.

ACKNOWLEDGEMENTS

This work was supported by the National Research Foundation of Korea (NRF) grant funded by the Korea government (MSIT) (Nos. 2019R1A2C2085583, 2020R1A5A1018153), the Korea Institute of Energy Technology Evaluation and Planning (KETEP), and the Ministry of Trade, Industry & Energy (MOTIE) of the Republic of Korea (Grant No. 20173010032170). S.K. acknowledges support from the research fund of Hanyang University (HY-202000000000524).

DATA AVAILABILITY STATEMENT

The data that supports the findings of this study are available in the supplementary material of this article.

ORCID

Wonjoon Choi https://orcid.org/0000-0002-1913-598X

REFERENCES

1. Zou Y, Raveendran V, Chen J. Wearable triboelectric nanogenerators for biomechanical energy harvesting. *Nano Energy*. 2020;77:105303.
2. Liu Y, Hu C. Triboelectric nanogenerators based on elastic electrodes. *Nanoscale*. 2020;12(39):20118-20130.
3. Liu W, Wang Z, Wang G, et al. Switched-capacitor-convertors based on fractal design for output power management of triboelectric nanogenerator. *Nat Commun*. 2020;11(1):1883.
4. Jing T, Xu B, Yang Y, Jiang C, Wu M. Interfacial modification boosted permittivity and triboelectric performance of liquid doping composites for high-performance flexible triboelectric nanogenerators. *Nano Energy*. 2020;78:105374.
5. Hwang HJ, Kim JS, Kim W, et al. An ultra-mechanosensitive visco-poroelastic polymer ion pump for continuous self-powering kinematic triboelectric nanogenerators. *Adv Energy Mater*. 2019;9(17):1803786.
6. Yin X, Liu D, Zhou L, et al. A motion vector sensor via direct-current Triboelectric Nanogenerator. *Adv Funct Mater*. 2020;30(34):2002547.
7. Niu S, Liu Y, Wang S, et al. Theoretical investigation and structural optimization of single-electrode Triboelectric Nanogenerators. *Adv Funct Mater*. 2014;24(22):3332-3340.
8. Seol M, Kim S, Cho Y, et al. Triboelectric series of 2D layered materials. *Adv Mater*. 2018;30(39):1801210.
9. Shin D, Seong T, Choi J, Choi W. Self-sustaining water-motion sensor platform for continuous monitoring of frequency and amplitude dynamics. *Nano Energy*. 2017;35:179-188.
10. Liu Y, Han R, Li L, Zhou Z, Chen G, Li Q. Tuning of highly dielectric calcium copper titanate nanowires to enhance the output performance of a triboelectric nanogenerator. *ACS Appl Electron Mater*. 2020;2(6):1709-1715.
11. Ferrie S, Darwish N, Gooding JJ, Ciampi S. Harnessing silicon facet-dependent conductivity to enhance the direct-current produced by a sliding Schottky diode triboelectric nanogenerator. *Nano Energy*. 2020;78:105210.
12. Seo B, Cha Y, Kim S, Choi W. Rational design for optimizing hybrid thermo-triboelectric generators targeting human activities. *ACS Energy Lett*. 2019;4(9):2069-2074.
13. Seo B, Hwang H, Kang S, Cha Y, Choi W. Flexible-detachable dual-output sensors of fluid temperature and dynamics based on structural design of thermoelectric materials. *Nano Energy*. 2018;50:733-743.
14. Wang ZL. Triboelectric nanogenerators as new energy technology and self-powered sensors – principles. *Probl Perspect Faraday Discuss*. 2014;176(0):447-458.
15. Zi Y, Guo H, Wang J, et al. An inductor-free auto-power-management design built-in triboelectric nanogenerators. *Nano Energy*. 2017;31:302-310.
16. Bhatia D, Lee J, Hwang HJ, Baik JM, Kim S, Choi D. Design of mechanical frequency regulator for predictable uniform power from triboelectric nanogenerators. *Adv Energy Mater*. 2018;8(15):1702667.
17. Cheng X, Miao L, Song Y, et al. High efficiency power management and charge boosting strategy for a triboelectric nanogenerator. *Nano Energy*. 2017;38:438-446.
18. Jiang T, Chen X, Han CB, Tang W, Wang ZL. Theoretical study of rotary freestanding triboelectric nanogenerators. *Adv Funct Mater*. 2015;25(19):2928-2938.
19. Ryu H, Yoon H-J, Kim S-W. Hybrid energy harvesters: toward sustainable energy harvesting. *Adv Mater*. 2019;31(34):1802898.
20. Liu D, Yin X, Guo H, Zhou L, Li X, Zhang C, Wang J, Wang ZL. A constant current triboelectric nanogenerator arising from electrostatic breakdown. *Science Advances*. 2019;5(4):eaav6437. http://dx.doi.org/10.1126/sciadv.aav6437.
21. Lee JH, Park YS, Cho S, Kang IS, Kim JK, Jeong U. Output voltage modulation in triboelectric nanogenerator by printed ion gel capacitors. *Nano Energy*. 2018;54:367-374.

22. Yang B, Zeng W, Peng Z-H, Liu S-R, Chen K, Tao X-M. A fully verified theoretical analysis of contact-mode triboelectric nanogenerators as a wearable power source. *Adv Energy Mater*. 2016;6(16):1600505.
23. Lin Z-H, Cheng G, Lee S, Pradel KC, Wang ZL. Harvesting water drop energy by a sequential contact-electrification and electrostatic-induction process. *Adv Mater*. 2014;26(27):4690-4696.
24. Zhu G, Lin Z-H, Jing Q, et al. Toward large-scale energy harvesting by a nanoparticle-enhanced triboelectric nanogenerator. *Nano Lett*. 2013;13(2):847-853.
25. Peng J, Kang SD, Snyder GJ. Optimization principles and the figure of merit for triboelectric generators. *Sci Adv*. 2017;3(12):eaap8576.
26. Ghaffarinejad A, Hasani JY, Hinchet R, et al. A conditioning circuit with exponential enhancement of output energy for triboelectric nanogenerator. *Nano Energy*. 2018;51:173-184.
27. Chen H, Xu Y, Zhang J, Wu W, Song G. Theoretical system of contact-mode triboelectric nanogenerators for high energy conversion efficiency. *Nanoscale Res Lett*. 2018;13:346.

SUPPORTING INFORMATION

Additional supporting information may be found online in the Supporting Information section at the end of this article.

How to cite this article: Seo B, Cha Y, Kim S, Choi W. Tunable current duration in triboelectric generators via capacitive air gaps. *Int J Energy Res*. 2021;45:5619–5628. https://doi.org/10.1002/er.6188